International Journal of Thermal Sciences 128 (2018) 70–83

Contents lists available at ScienceDirect

International Journal of Thermal Sciences

journal homepage: www.elsevier.com/locate/ijts

Thermal and hydraulic numerical study for a novel multi tubes in tube helically coiled heat exchangers: Effects of operating/geometric parameters

H.F. Elattar[a,*], A. Fouda[b], S.A. Nada[a], H.A. Refaey[c], A. Al-Zahrani[d]

[a] Department of Mechanical Engineering, Benha Faculty of Engineering, Benha University, Benha, 13511 Qalyubia, Egypt
[b] Department of Mechanical Power Engineering, Faculty of Engineering, Mansoura University, 35516 El-Mansoura, Egypt
[c] Department of Mechanical Engineering, Faculty of Engineering at Shoubra, Benha University, 11629 Cairo, Egypt
[d] Department of Mechanical Engineering, Faculty of Engineering, University of Jeddah, 21589 Jeddah, KSA

A R T I C L E I N F O

Keywords:
Helical coil
Multi tubes in tube
Heat exchanger
CFD simulation
Thermal-hydraulic performance

A B S T R A C T

Compactness with high performance heat exchangers are main challenges in a lot of engineering applications. Thus, this research reports CFD simulation of a novel MTTHC (multi tubes in tube helically coiled) heat exchanger using ANSYS-FLUENT 14.5. The aim of the work is to investigate the thermal and hydraulic performance of the MTTHC for turbulent flow. The effects of the operating and geometrical parameters of the coil on the cold/hot water Nusselt numbers, heat transfer coefficients, pumping power, effectiveness, and thermal-hydraulic index are studied and presented. The results show that, the largest heat transfer coefficient is found at $N = 3$ and $\beta = 0^\circ$ & 90°, and the pumping power (P) rises with ≅20 times if N changed from 1 to 5 at any β. Moreover, the effectiveness of the coil (ε) has the largest values at $\beta = 0^\circ$ & 90° and $N=3$, and it enhances with 8.5%, 9% and 7% if N increased from 1 to 3 at $\beta = 0^\circ$, 45° and 90°, respectively. In addition, thermal-hydraulic index (ξ) improves with 5%, 8% and 6% if N increased from 1, to 3 at $\beta = 0^\circ$, 45° and 90°, respectively. Finally, Numerical correlations for P, ε and ξ are correlated and presented within reasonable errors.

1. Introduction

Heat exchangers in the shape of helical coils are broadly used in several engineering applications such as energy conversion systems, refrigeration and air conditioning systems, chemical processing, thermal power plants, nuclear reactors, solar energy concentrator receivers, and medical equipment, due to their higher thermal performance and compact size. The flow field and the overall heat transfer coefficient in a helically coiled tube are complex as compared with the conventional heat exchanger and this is due to the dependence of the secondary flow behavior on curvature of tubes. Furthermore, a centrifugal force is generated within fluid flow because of the curvature of the tubes, so the rate of heat transfer is enhanced significantly as the induced of secondary flow. Double tubes and shell and tube helically coils heat exchangers were numerically and experimentally investigated. Owing to the complication of studying the heat transfer processes and fluid flow field in the helically coiled tubes heat exchangers, experimental investigations are costly, limited study parameter ranges and consuming time and the numerical investigations are replacement tool by using CFD packages for this concern.

The Effects of the Prandtl number and geometrical parameters on both the average and local Nusselt numbers for flow in helical pipes was investigated experimentally by Xin and Ebadian [1]. New empirical correlations for the average Nusselt number have been regressed and presented and no noticeable effect of the coil pitch existed. Xin et al. [2] investigated experimentally the effects of the coil geometry and fluid flow rates for both single-phase and two-phase (air/water) flow on helical annular pipes pressure drop for vertical and horizontal coil orientations. Different pressure drop correlations for single-phase and two-phase flow were established and presented. Rennie and Raghavan [3] reported experimentally the heat transfer in a double-pipe heat exchanger comprised one loop. Two heat exchangers with different sizes for both parallel and counter flow configurations were examined. The heat transfer coefficients in the inner tube and the annulus were obtained with different fluids flow rates. A small difference between the overall heat transfer coefficients for the parallel flow and counter flow configurations were found in spite of the higher heat transfer rates that appeared in counter flow configuration. Kumar et al. [4] performed experimental and numerical studies of tube-in-tube helical heat exchanger at the pilot plant scale. The hydrodynamics and heat transfer characteristics were investigated with different inner tube and annulus mass flow rates for counter flow configuration. A commercial CFD package (FLUENT 6.0) was used to predict the flow and thermal profiles in the coil. It was found that the overall heat transfer coefficient

* Corresponding author.
E-mail address: hassan.alattar@bhit.bu.eud.eg (H.F. Elattar).

https://doi.org/10.1016/j.ijthermalsci.2018.02.020
Received 14 October 2017; Received in revised form 25 January 2018; Accepted 19 February 2018
1290-0729/

Nomenclature

A_o	Cross sectional area of annulus $A_o = \pi(D^2 - N\ d_o^2)/4$, m^2
A_i	Cross section area of inner tubes, $A_i = \frac{\pi}{4}Nd_i^2$, m^2
Bo_i	Hot water buoyancy parameter, $Bo_i = \frac{Gr_i}{\mathrm{Re}_i^{3.5}\mathrm{Pr}_i^{0.8}}$
Bo_o	Cold water buoyancy parameter, $Bo_o = \frac{Gr_o}{\mathrm{Re}_o^{3.5}\mathrm{Pr}_o^{0.8}}$
C_o	Cold water heat capacity, $C_o = \dot{m}_o C_{p,o}$, W/K
C_i	Hot water heat capacity, $C_i = \dot{m}_i C_{p,i}$, W/K
$C_{p,o}$	Cold water average specific heat, J/kg.K
$C_{p,i}$	Hot water average specific heat, J/kg.K
D	Outer tube diameter, m
D_c	Diameter of helical coil, m
De_i	Hot water Dean number, $De_i = \mathrm{Re}_i\sqrt{\frac{d_i}{D_c}}$
De_o	Cold water Dean number, $De_o = \mathrm{Re}_o\sqrt{\frac{D_h}{D_c}}$
D_h	Annulus hydraulic diameter, $D_h = \frac{4A_o}{\pi(D+\ N\ d_o)}$, m
d_i	Internal diameter of inner tubes, m
d_o	External diameter of inner tubes, m
H	Coil pitch, m
h_i	Hot water average heat transfer coefficient, W/m^2.K
h_o	Cold water average heat transfer coefficient, W/m^2.K
K_o	Cold water average thermal conductivity, W/m.K
K_i	Hot water average thermal conductivity, W/m.K
L	Length of helical coil, $L = Z(H^2 + (\pi D_c)^2)^{0.5}$, m
$\dot{m}_o$	Cold water mass flow rates, $\dot{m}_o = \rho_o v_o A_o$, kg/s
$\dot{m}_i$	Hot water mass flow rates, kg/s
Nu_o	Cold water average Nusselt number
Nu_i	Hot water average Nusselt number
N	Inner tubes number
Pr_i	Hot water Prandtl number
Pr_o	Cold water Prandtl number
$\dot{Q}_o$	Cold water heat transfer rates $\dot{Q}_o = C_o\Delta t_o$, W
$\dot{Q}_i$	Hot water heat transfer rate, $\dot{Q}_i = C_i\Delta t_i$, W
$\dot{Q}_{avg}$	Average heat transfer rate, W
P	Pumping power of the coil, W
Re_i	Hot water Reynolds number, $\mathrm{Re}_i = \frac{\rho_i v_i d_i}{\mu_i}$
Re_o	Cold water Reynolds number, $\mathrm{Re}_o = \frac{\rho_o v_o D_h}{\mu_o}$
$Re_{cr,o}$ $T_{s,avg}$	Critical Reynolds number of cold side, $\mathrm{Re}_{cr,o} = 2000\left(\frac{d_i}{D_c}\right)^{0.32}$
$Re_{cr,i}$ $T_{s,avg}$	Critical Reynolds number of hot side, $\mathrm{Re}_{cr,i} = 2000\left(\frac{D_h}{D_c}\right)^{0.32}$
$t_{s,avg}$	Inner tubes average surface temperature, °C
$t_{o,avg}$	Cold water average temperature, °C
$t_{i,avg}$	Hot water average temperature, °C
$t_{o,in}$	Temperature of inlet cold water, °C
$t_{o,out}$	Temperature of outlet cold water, °C
$t_{i,in}$	Temperature of inlet hot water, °C
$t_{i,out}$	Temperature of outlet hot water, °C
U_o	Overall heat transfer coefficient, W/m^2.K
Z	Number of coil turns
ΔP_o	Cold water pressure drop, Pa
ΔP_i	Hot water pressure drop per inner tube, Pa
$\Delta P_{i,\ avg}$	Hot water average pressure drop for all inner tubes, $\Delta P_{i,avg} = \frac{\sum \Delta P_i}{N}$, Pa
$\Delta t_{i,s,avg}$	Temperature difference between the surface temperature of the inner tubes and the average hot water temperature, $\Delta t_{i,s,avg} = t_{i,avg} - t_{s,avg}$, °C
$\Delta t_{o,s,avg}$	Temperature difference between the surface temperature of the inner tubes and the average cold water temperature, $\Delta t_{o,s,avg} = t_{s,avg} - t_{o,avg}$, °C
Gr_i	Hot water Grashof number, $Gr_i = \frac{g\beta_i(t_{i,avg} - t_{s,avg})d_i^3}{\nu_i^2}$
Gr_o	Cold water Grashof number, $Gr_o = \frac{g\beta_o(t_{s,avg} - t_{o,avg})D_h^3}{\nu_o^2}$

Greek symbols

β_i	Coefficient of volume expansion of hot water, (1/K)
β_o	Coefficient of volume expansion of cold water, (1/K)
ε	effectiveness of the coil
μ_w	Water dynamic viscosity, Pa.s
ν_i	Hot water kinematic viscosity, (m^2/s)
ν_o	Cold water kinematic viscosity, (m^2/s)
ρ_w	Water density, kg/m^3
ξ	Thermal-hydrodynamic performance index [W/Pa]

increases with increasing the Dean number in the inner-coiled tube for a constant annulus flow rate. Kumar et al. [5] studied numerically tube-in-tube helically coiled (TTHC) heat exchanger using renormalization group (RNG) k–ε model for modeling the turbulent flow and heat transfer. The fluid flow and heat transfer characteristics were investigated for different inner (compressed air) and outer (cooling water) tube fluid flow rates for both parallel and counter flow configurations. New empirical correlations for the hydrodynamic and the heat-transfer were developed. Jayakumar et al. [6] presented experimental and CFD (Fluent 6.2) theoretical analysis of a helically coiled heat exchanger considering fluid-to-fluid heat transfer. The effects of the actual fluid properties instead of constant values on the heat transfer characteristics were presented and empirical correlation for inner heat transfer coefficient was developed. Piazza and Ciofalo [7] predicted numerically the turbulent flow and heat transfer in helically coiled heat exchangers using the k–ε, SST k–ω and RSM–ω that compared with DNS results and experimental data available of pressure drop and heat transfer. It was observed that the standard k–ε model, with a near-wall treatment presents under prediction of both friction coefficient and Nusselt number. Colorado et al. [8] carried out numerical study and experimental validation to describe the heat transfer and fluid dynamic behavior of a helically coiled steam generator using transient analysis one dimensional model. The proposed model includes subcooled liquid, two-phase flow, and superheated vapour regions. Zhou et al. [9] developed a novel thermodynamic optimization model based on minimizing the work loss for tube-in-tube helically coiled heat exchangers. The effects of main design parameters of the heat exchanger on the available work loss were discussed and presented and the optimal design parameters were also obtained. The results of optimization model provided useful guidance for using such heat exchangers in Joule-Thomson refrigerators. Nada et al. [10] conducted an experimental study of the performance and compactness enhancement of helical-coil in a shell by the attachment of radial fins on the outer surface of the coils. Experimental correlations of Nusselt number in terms Re, Gr, and shell diameter were developed for finned and unfinned coils. Amori [11] investigated experimentally the thermo-fluid characteristics of helically coiled heat exchanger immersed in cold water. Two types of coils were tested; a conventional vertical coil and a new triple vertical coil in parallel connection i.e. meshed coils. The effect of hot water flow rates inside the tubes that varied from 2.67 to 7.08 l/min, and the inlet temperatures, namely 50, 60, 70 and 80 °C were tested. Enhancements of heat transfer and pumping power saving for meshed coils compared to single coil were notices.

Nada et al. [12–14] and Fouda et al. [15] investigated experimentally and numerically the heat transfer and pressure drop characteristics in annulus formed by multi hot rods in tube helically coiled heat exchanger for laminar flow. The effects of the geometric parameters and fluid flow parameters; number of inner tubes, annulus hydraulic diameter, Reynolds numbers and input heat flux on coil performance were discussed. It was observed that the coil with three inner rods had the best heat transfer characteristics and average Nusselt number. Empirical correlations were developed in terms of Reynolds number, Prandtl number and coil hydraulic diameter. Pawar and Sunnapwar [16] carried out experimental study and CFD simulation using FLUENT 12.0.16 commercial package on isothermal steady state and non-isothermal unsteady state conditions in helical coils for Newtonian and non-Newtonian fluids. The correlations for Nusselt number and friction factor were developed for laminar and turbulent flow for both Newtonian and non-Newtonian fluids. Pan et al. [17] investigated numerically the heat transfer and pressure drop for oscillating flow in helically coiled tube heat-exchanger using CFD code Fluent. The average Nusselt number and average pressure drop correlations were proposed with taking into account the flow frequency and its inlet velocity. Hardik et al. [18] studied experimentally the influence of curvature i.e. coil to tube diameter ratio, Reynolds number and Prandtl number on local Nusselt number and friction factor in a helical coil with water as the working fluid. Correlations for fully developed overall averaged inner side, outer side and total Nusselt numbers were presented. Sartori et al. [19] presented and validated 3D-CFD simulation model of helically coiled tube flocculators (HCTFs) to evaluate the influence of changing reactor diameter and operating flow rate on the distributions of velocity gradient, axial velocity and secondary flow structures. Numerical correlation was obtained to aid the reasonable design of HCTFs by describing the variation of the mean velocity gradient in terms of Reynolds number and the ratio between the curvature and torsion. Pawar et al. [20] carried out experimental work using water, 10 and 20% glycerol–water mixture as Newtonian fluids. The experiments were accomplished using four helical coils with different coil curvature ratios for laminar and turbulent flow regimes. It was detected that Nusselt number decreases with increasing the helical coil diameter due to the decrease in the centrifugal force. Bahremand et al. [21] investigated numerically and experimentally the turbulent flow in helically coiled tubes under constant wall heat flux. Convective heat transfer coefficient and pressure drop of water and water–silver nanofluid is examined. The numerical computations are achieved by Eulerian–Lagrangian two-phase approach in connection with an RNG k–ε turbulence model using ANSYS CFX software. Two correlations were developed to predict the ratio of the mean heat transfer coefficient and the pressure drop of nanofluid to water in helical tubes. It was observed that these ratios are independent of Reynolds number; however the curvature ratio affects these ratios.

Zheng et al. [22–25] studied experimentally and numerically the heat transfer performance of a high-density polyethylene helical coil heat exchanger (HCHE) which is adopted by a seawater-source heat pump system (SWHP). The effects of inlet temperature, intermediate medium velocity, pipe length and diameter, temperature of seawater and icing outside the pipes on the heat transfer performance of the HCHE are investigated. Moreover, the effects of seawater flow rate are also investigated and a correlation between Nusselt and Reynolds number is presented.

Although extensive work has been published on flow and heat transfer characteristics in helical/curved pipes and in annulus of double pipe helical heat exchangers, no data are available in literature for turbulent flow in multi tubes in tube helically coiled heat exchangers. While multi tubes in tube helically coiled (MTTHC) heat exchangers are desirable in a lot of engineering applications, fluid flow and heat transfer characteristics of such type of heat exchangers are not published yet. However, the detailed characteristics of fluid flow and heat transfer inside helical coil is not available from the present literature.

Consequently, the novelty of this work is primarily to present the thermal and hydraulic performance of MTTHC heat exchangers as novel compacted heat exchangers under various coil geometric and operating parameters. Accordingly, the present study aims to investigate numerically the thermal and hydraulic performance; cold/hot water Nusselt numbers, heat transfer coefficients, pumping power, effectiveness, and thermal-hydraulic index of MTTHC heat exchangers for turbulent flow. Influences of coil geometric parameters; number of inner tubes, coil inclination angle and coil operating parameters; cold/hot

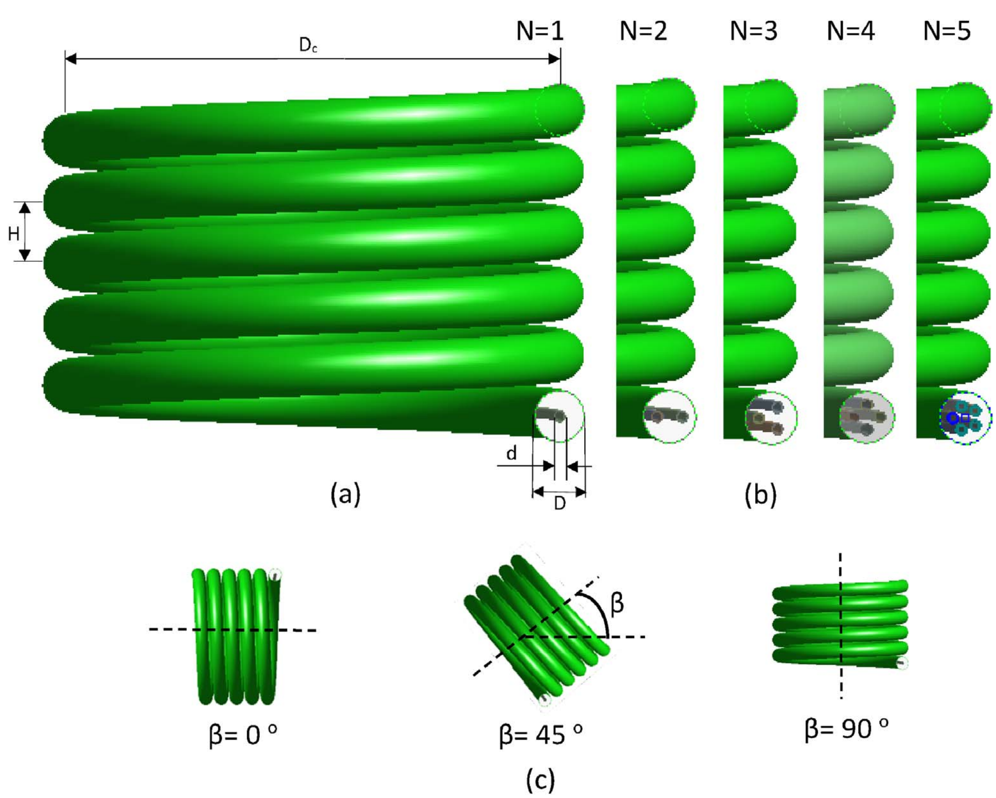

Fig. 1. Physical model: (a) geometry of MTTHC, (b) inner tubes configuration (c) coil orientations.

water Reynolds/Dean numbers and temperatures on the coil thermal and hydraulic performance are studied, discussed and presented. Moreover, new numerical correlations for MTTHC heat exchanger performance are presented.

2. Modeling of MTTHC heat exchangers

The MTTHC heat exchangers that modeled numerically consists of one/multi coiled tubes, placed inside and outer helical coil. In the present study, the hot fluid flows in the inner tubes, while the cold fluid flows in the annulus region in counter flow configuration. The simulation tool, ANSYS-FLUENT 14.5 CFD commercial package is used and the governing equations are solved for flow, temperature and pressure values for each cell.

The geometry used for CFD modeling of MTTHC heat exchangers with one/multi inner tubes arrangements are shown in Fig. 1. The coils are constructed from one/multi inner tubes arranged in circular shape inside the helically outer tube. The coils are modeled in the counter flow configuration, where the cold fluid (water) flows in the annulus space with inlet temperature, t_i = 15 & 25 °C while the hot fluid flows in the inner tube/tubes with inlet temperature, t_o = 40 & 50 °C. The inner (d_i) and outer (d_o) diameters of the inner tube are 5 mm and 5.5 mm, respectively. The outer coil tube diameter (D), length (L) and tube thickness (δ) are 25 mm, 3.93 *m*, and 0.25 mm, respectively and the inner tubes are arrayed equally inside it. The outer tube and inner tubes are coiled together to form MTTHC heat exchanger with coil diameter, Dc = 250 mm, coil pitch, H = 30 mm, and the number of coil turns, Z = 5. Five numbers of inner tube/tubes; N = 1, 2, 3, 4 and 5 and three coil inclination angles, β = 0° (horizontal), 45°, and 90° (vertical) are simulated.

3. Mathematical formulation and computational methodology

3.1. Governing equations and numerical method

In the numerical simulation, the three-dimensional time-averaged governing equations of turbulent flow and heat transfer in MTTHC heat exchanger in Cartesian coordinate system (x, y, z) are applied in this study. The current study indicates a flow in MTTHC where there is a rotation of flow because of the construction of the helical coils. The Realizable k-ε turbulence model is applied for modeling the heat transfer and turbulent flow because it precisely expects the curved and swirled flow as compared with other k-ε models and it offers also higher performance for computational time [26]. Moreover, the Realizable k-ε comprises a new formulation for the realizable eddy viscosity and new transport equation for the dissipation rate, which was resultant from the transport equation of average square vorticity fluctuation. Additionally, the Realizable k-ε illustrates a higher capability to capture the average flow of the compound structures. The time-averaged governing equations in three-dimensional form for turbulent flow and heat transfer in *MTTHC* heat exchanger are presented in master Cartesian tensor form as follows:

$$\frac{\partial U_i}{\partial x_i} = 0 \tag{1}$$

$$\rho U_i \frac{\partial U_i}{\partial x_i} = -\frac{\partial P}{\partial x_j} + \frac{\partial}{\partial x_i}\left[\mu\left(\frac{\partial U_i}{\partial x_j} + \frac{\partial U_j}{\partial x_i}\right) - \rho\overline{u'_i u'_j}\right] \tag{2}$$

$$\rho c_p U_i \frac{\partial T}{\partial x_i} = \frac{\partial}{\partial x_i}\left[\lambda\frac{\partial T}{\partial x_j} - \rho c_p \overline{u'_i T'}\right] \tag{3}$$

$$\frac{\partial}{\partial t}(\rho k) + \frac{\partial}{\partial x_j}(\rho k u_j) = \frac{\partial}{\partial x_j}\left[\left(\mu + \frac{\mu_t}{\sigma_k}\right)\frac{\partial k}{\partial x_j}\right] + G_k + G_b - \rho\varepsilon - Y_M + S_k \tag{4}$$

$$\frac{\partial}{\partial t}(\rho\varepsilon) + \frac{\partial}{\partial x_j}(\rho\varepsilon u_j) = \frac{\partial}{\partial x_j}\left[\left(\mu + \frac{\mu_t}{\sigma_\varepsilon}\right)\frac{\partial \varepsilon}{\partial x_j}\right] + \rho C_1 S\varepsilon - \rho C_2\frac{\varepsilon^2}{k + \sqrt{\nu\varepsilon}} + C_{1\varepsilon}\frac{\varepsilon}{k}C_{3\varepsilon}G_b + S_\varepsilon \tag{5}$$

where, t and U_i are the time-averaged temperature and velocity. *P,* ρ, μ, *R,* and λ are static pressure, density, viscosity, gas constant and thermal diffusivity, respectively.$\rho c_p\overline{u'_i T'}$, $-\rho\overline{u'_i u'_j}$, u'_i, u'_j and T' are the turbulent heat fluxes, average Reynolds stresses, the fluctuating velocities and temperature, respectively. The coefficients of simulation model are $\sigma_\kappa = 1.0$, $\sigma_\varepsilon = 1.2$, $C_2 = 1.9$, $C_{1\varepsilon} = 1.44$ and G_k and G_b are generation of turbulence kinetic energy due to the average velocity gradients and buoyancy, respectively, where Y_M indicates the contribution of the fluctuating dilatation in compressible turbulence to the overall dissipation rate, and μ_t is the turbulent viscosity. In the current simulation, the turbulent intensity is selected as 5% for cold/hot fluids inlets based on average Reynolds number for the studied ranges. The governing equations are discretized by using second order upwind interpolation scheme utilized by ANSYS-FLUENT and the SIMPLE algorithm is chosen for pressure velocity coupling. To assert precise results, the solution is considered to be converged when variables in domain versus iteration seem to be constant, and the normalized residual of continuity, momentum, and energy are less than 10^{-4}, 10^{-5} and 10^{-6}, respectively.

3.2. Boundary conditions, studied parameters and mesh generation

The boundary conditions of the studied domain are selected as follows: the hot/cold fluid flow in the coil is turbulent flow; the distributed uniform axial velocity and temperature are assumed at the inlets of the inner tubes and annulus, while at the outlets the zero pressure conditions. No slip conditions are imposed at the inner and outer tubes surfaces. In the present simulation, the studied parameters ranges are tabulated in Table 1, the tubes are made of cupper (ρ = 8978 kg/m^3, C_p = 381 J/kg.K and k = 387.6 W/m.K) and assumed to be smooth and the coil outside surface is selected to be adiabatic during the simulation. The grid is generated with hexahedral and wedges elements as shown in Fig. 2. To verify the independence of the present numerical simulation on the grid size, a mesh independence study is performed by calculating the temperature difference of hot and cold water through the heat exchanger with different number of cells as illustrated in Fig. 3.

The mesh independence study showed that the fluctuation between the calculated parameters using the studied grids decreases with increasing the number of cells, and these fluctuations are not more than 2% above cell number of 1171448, 1045644, 1050979, 1121757 and 902090 at N = 1, 2, 3, 4 and 5 respectively, and at Re_i = 9000, Re_o = 17000, t_i = 50 °C and t_o = 25 °C as illustrated in Fig. 3. So, these numbers of cells are considered as grid independence and used to fulfill the present simulations.

Table 1
Studied parameters ranges.

Studied parameter	Values
Cold water temperature, t_o	15 & 25 °C
Hot water temperature, t_i	40 & 50 °C
Cold water Reynolds number, $R_{e,o}$	From 9000 to 17000
Hot water Reynolds number, $R_{e,i}$	From 14000 to 22000
Cold water Dean number, De_o	From 3177 to 4992
Hot water Dean number, De_i	From 1273 to 2404
Number of inner tubes, N	1, 2, 3, 4 and 5
Coil inclination angle, β	0°, 45°, and 90°

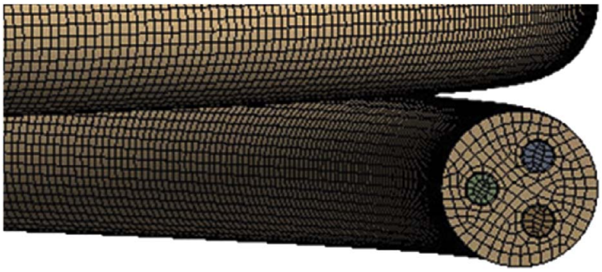

Fig. 2. Grid of MTTHC

3.3. Thermal and hydraulic performance parameters of MTTHC heat exchanger

According to the temperature results obtained from numerical simulation models for all studied coils, the coils heat transfer characteristics, thermal performance, and thermal-hydraulic index can be calculated and presented as follows.

The overall heat transfer coefficient based on outside surface of inner tubes and consequently the number of transfer units, NTU can be calculated in the following forms:

$$U_o = \frac{Q^{\bullet}_{avg}}{\pi N L d_o \Delta t_{LMTD}} \tag{6}$$

$$NTU = \frac{\pi N L d_o U_o}{C_{\min}} \tag{7}$$

$$Q^{\bullet}_{avg} = \frac{Q^{\bullet}_i + Q^{\bullet}_o}{2} \tag{8}$$

$$\Delta t_{LMTD} = \frac{\Delta t_1 - \Delta t_2}{\ln\left(\frac{\Delta t_1}{\Delta t_2}\right)} \tag{9}$$

Where

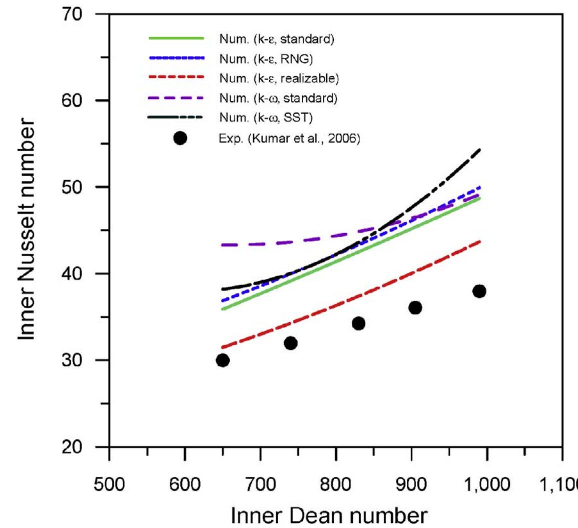

Fig. 4. Turbulence models comparison and validation.

$$C_{\min} = min(C_c \& C_h)$$

$$\Delta t_1 = t_{i,in} - t_{o,out}$$

$$\Delta t_2 = t_{i,out} - t_{o,in}$$

The average heat transfer coefficients and Nusselt numbers for hot and cold water flows are given as follows:

$$\bar{h}_i = \frac{Q^{\bullet}_{avg}}{\pi d_i L N \Delta t_{i,s,avg}} \tag{10}$$

$$\bar{h}_o = \frac{Q^{\bullet}_{avg}}{\pi d_o L N \Delta t_{o,s,avg}} \tag{11}$$

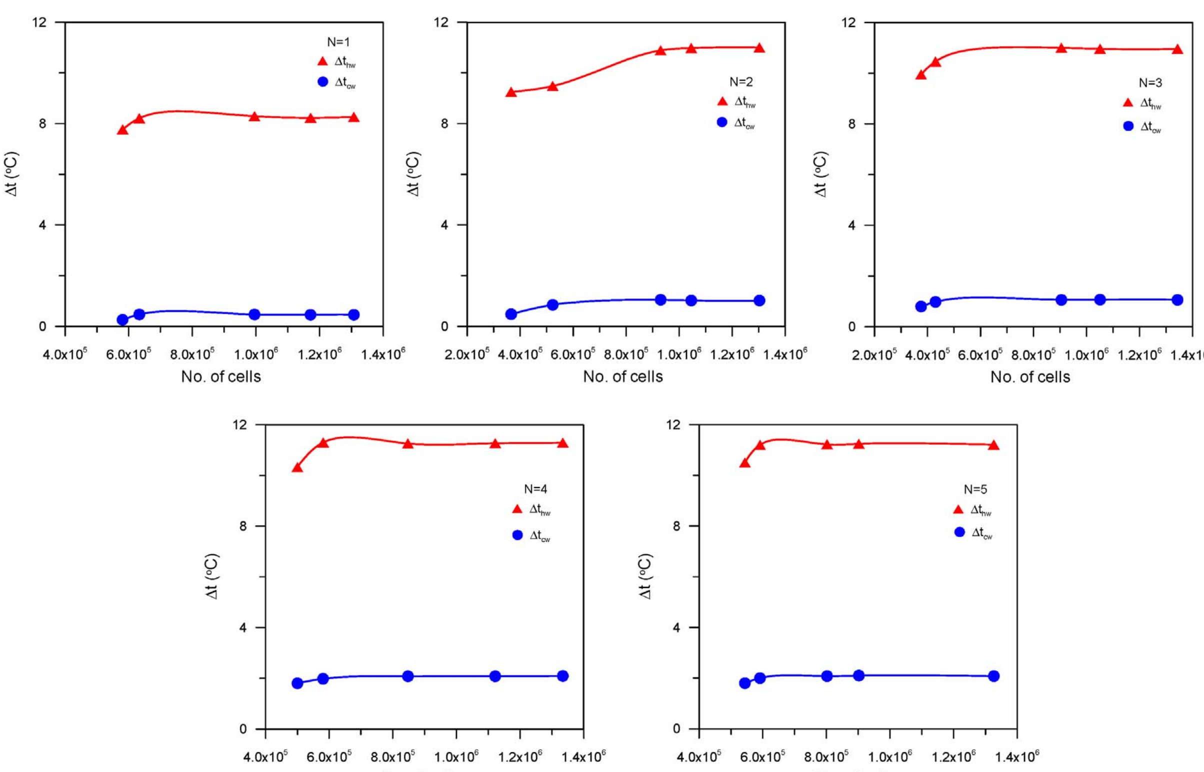

Fig. 3. Mesh independence study.

Table 2
Summary of simulation cases in the present work.

	Group 1	Group 2	Group 3	Group 4	Group 5	Group 6
Studied parameters	t_o = 15 °C, t_i = 40 °C, $\beta = 0°$	t_o = 15 °C, t_i = 50 °C, $\beta = 0°$	t_o = 25 °C, t_i = 40 °C, $\beta = 0°$	t_o = 25 °C, t_i = 50 °C, $\beta = 0°$	t_o = 25 °C, t_i = 50 °C, $\beta = 45°$	t_o = 25 °C, t_i = 50 °C, $\beta = 90°$
	$Re_o = 14 \times 10^3$, 16×10^3, 18×10^3, 20×10^3 and 22×10^3 $Re_i = 9 \times 10^3$, 11×10^3, 13×10^3, 15×10^3 and 17×10^3 N = 1, 2, 3, 4 and 5					
No. of runs	125	125	125	125	125	125

$$Nu_i = \frac{\bar{h}_i d_i}{k_{i,avg}} \tag{12}$$

$$Nu_o = \frac{\bar{h}_o D_h}{k_{o,avg}} \tag{13}$$

The effectiveness and thermal-hydraulic index can be determined as follows:

$$\varepsilon = \frac{\dot{Q}_{avg}}{\dot{Q}_{\max}} \tag{14}$$

$$\xi = \frac{\dot{Q}_{avg}}{\Delta P_o + \sum \Delta P_i} \tag{15}$$

Where

$$\dot{Q}_{\max} = C_{\min} \Delta t_{\max}$$

$$\Delta t_{\max} = t_{i,in} - t_{o,in}$$

The friction factor for hot and cold-water sides and pumping power are calculated from the following formulas:

$$f_i = \frac{2 d_i \Delta P_{i,avg}}{L \rho_i v_i^2} \tag{16}$$

$$f_o = \frac{2 D_h \Delta P_o}{L \rho_o v_o^2} \tag{17}$$

$$P = \dot{m_o} \frac{\Delta P_o}{\rho_o} + \dot{m_i} \frac{\sum \Delta P_i}{\rho_i} \tag{18}$$

For the sake of accurate results, fluid properties were not assumed to be constant but they are analyzed and calculated as temperature dependent properties as given by the following correlations [27].

$$\rho(t) = 999.98 + 4.69 \times 10^{-2} t - 7.54 \times 10^{-3} t^2 + 4.36 \times 10^{-5} t^3 - 1.46 \times 10^{-7} t^4 \tag{19}$$

$$k(t) = 0.547 + 2.05 \times 10^{-3} t - 4.71 \times 10^{-6} t^2 - 8.89 \times 10^{-8} t^3 + 4.81 \times 10^{-10} t^4 \tag{20}$$

$$\mu(t) = 1.77 \times 10^{-3} - 5.49 \times 10^{-5} t + 9.93 \times 10^{-7} t^2 - 9.44 \times 10^{-9} t^3 + 3.55 \times 10^{-11} t^4 \tag{21}$$

$$C_p(t) = 4.23 - 7.15 \times 10^{-3} t + 4.42 \times 10^{-4} t^2 - 1.32 \times 10^{-5} t^3 + 2.03 \times 10^{-7} t^4 - 1.53 \times 10^{-9} t^5 + 4.53 \times 10^{-12} t^6 \tag{22}$$

Where, t is the temperature in °C.

The above equations from 6 to 22 are programmed and solved using EES (Engineering Equation Solver) software based on the results obtained from the numerical simulation models as the dependent parameters.

3.4. Model validation

In the present work, studies for proper turbulence model selection and model validation were carried out using different turbulence models and their results were compared to available experimental data in the literature as illustrated in Fig. 4. The turbulence models are selected and verified by comparing the predicted value of experimental Nusselt number in the inner tubes presented by Kumar et al. [4] with the present numerical simulations. The simulation was performed for N = 1, d = 0.0254 m, $D = 0.0508\,m$, $D_c = 0.762\,m$, $H = 0.100\,m$, $Z = 4$, $t_{cw} = 27$ °C, $t_{hw} = 50$ °C, $Re_{hw} = 3100$–5700, $Re_{cw} = 21000$–35000, and with 3,625,685 number of cells based on the Kumer's data that considered to be closest experimental data to current study.

As shown in Fig. 4, the numerical simulation using realizable k-ε turbulent model gives preferable results with the published experimental data compared to other turbulence models with maximum error of 15%. This discrepancy is due to the difference in the boundary conditions, numerical assumptions and experimental uncertainties. As a result, the realizable k-ε turbulence model gives satisfactory agreement results with experimental data, therefore it is recommended to achieve the present simulation.

4. Results and discussions

A full-matrix of results was produced based on six groups of simulation cases, each group including five values of Re_o (14×10^3, 16×10^3, 18×10^3, 20×10^3 and 22×10^3), five values of Re_i (9×10^3, 11×10^3, 13×10^3, 15×10^3 and 17×10^3) and five values of N (1, 2, 3, 4 and 5) with maintaining constant values of ti, t_o, and β to obtain 125 simulation cases for each group and for a total 750 simulation cases for all groups. The summary of simulation cases in the present work are summarized in Table 2. The simulation cases for studying the effects of coil geometrical and operational parameters in addition to the coil orientation on the thermal and hydraulic coil performance and pumping power are presented and discussed in details in the following sections.

4.1. Effects of hot/cold water dean numbers, temperatures, and Reynold's numbers

The influences of hot/cold Dean numbers and water temperatures, t_i & t_o on Nu_i, Nu_o, f_i, f_o, P, ε and ξ are illustrated in Fig. 5 (a) - (j). As shown in Fig. 5 (a) and (b), Nu_i and Nu_o increase with increasing De_i and De_o, respectively, the trends are the same for any values t_i & t_o. This can be attributed to the increase of De_i and De_o, i.e. the same effects of Re_i and Re_o since D_c, d and N are fixed, that leads to increasing the turbulence level and heat transfer rate which causes an enhancement to the heat transfer coefficients and consequently Nusselt numbers. Moreover, it can be seen from Fig. 5 (a) and (b) that Nu_i and Nu_o increase with decreasing hot/cold water temperatures (t_i and t_o) and this is due to increasing the heat transfer rate with increasing the temperature difference between the hot and cold water streams. Whereas, Fig. 5 (c) and (d) display that fi and f_o decrease with increasing De_i and De_o. This owing to increasing the hot/cold water velocities prevails the raise of the pressure drop, ΔP with De, so friction factor reduces with higher De. Moreover, Fig. 5(a) and (b) reveals that f_i and f_o decrease with increasing t_i and t_o at any De_i and De_o, respectively. This is

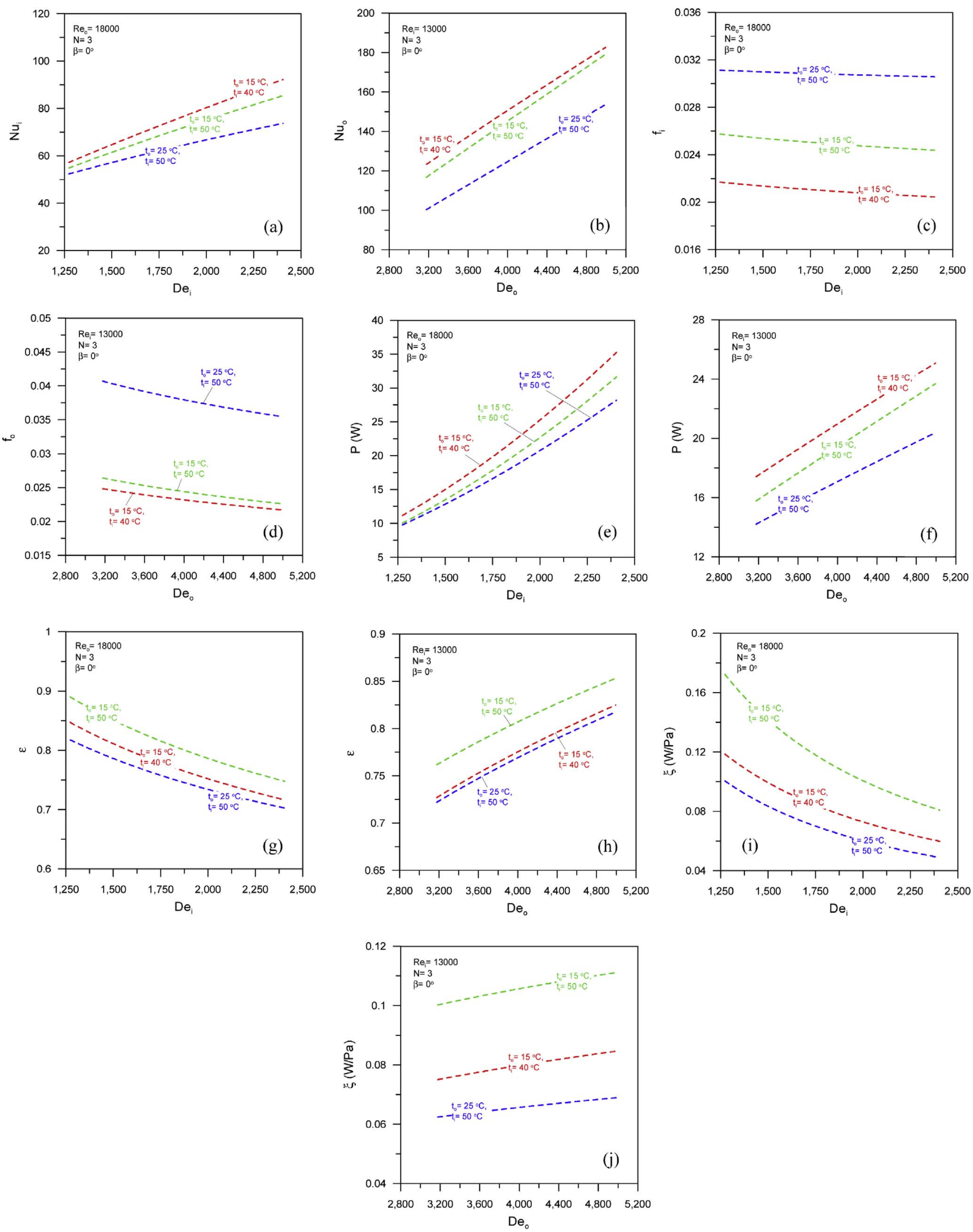

Fig. 5. Effect of hot/cold water Dean.

because of decreasing the hot/cold water densities and dynamic viscosities that leads to decreasing the water velocities to maintain constant Reynold's number, i.e. constant De and reduces also ΔP. Where, the drop in hot/cold water velocities overcome the drop in ΔP, thus the lower f_i and f_o can be attained with increasing t_i and t_o, respectively.

Fig. 5 (e)-(f) shows that P increases with increasing De_i and De_o and

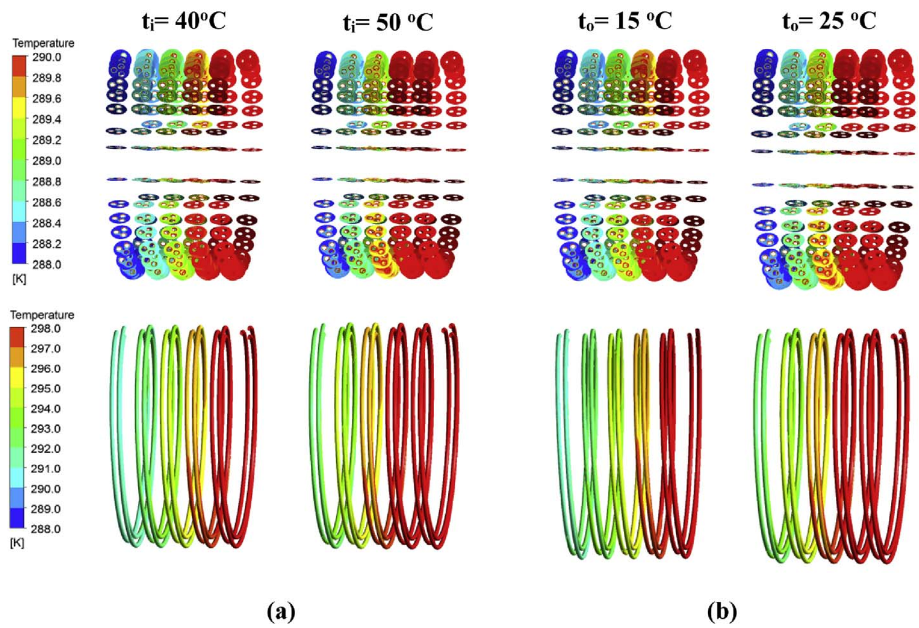

Fig. 6. Temperature contours at different: (a) hot water temperature at t_o = 15 °C (b) cold water temperature at t_i = 50 °C.

this is due to increasing the hot and cold water mass flow rates and pressure drops with increasing De_i and De_o. Moreover, P decreases with decreasing t_o and t_i, and this is attributed to the decreasing of the viscosity of hot and cold water with increasing t_i and t_o, and consequently a reduction of hot and cold water pressure drops can be appeared. For example, P decreases by 8% & 14% with increasing t_o from 15 °C to 25 °C and with 14% & 8% with increasing t_i from 40 °C to 50 °C for De_i = 1838 and De_o = 4085, respectively.

Fig. 5 (g) - (j) shows that, ε and ξ decrease and increase with increasing De_i and De_o, respectively and the trends are the same for any t_i & t_o. Decreasing ε with De_i as shown in Fig. 5 (g) can be attributed to the increase of the heat capacity of hot water (C_{min}) with increasing De_i which leads to the increase of $Q^{\bullet}_{max}$ and consequently lower ε can be revealed. The increase of ε with De_o is shown in Fig. 5(h) which owing to the increase of the overall heat transfer coefficient (U_o) that causes an increase in the heat transfer rate. On the other side, the decrease of ξ with De_i (as shown in Fig. 5 (i)) is attributed to the increase of the hot and cold water pressure drops which dominates the increase in the average rate of heat transfer, and vice versa as displayed in Fig. 5(j). Additionally, Fig. 5 (g) - (j) shows that ε and ξ improve with decreasing t_o and increasing t_i. The increase of ε and ξ with decreasing t_o and increasing t_i are attributed to the increase of the average heat transfer rate as a result to increasing the temperature difference between hot and cold flow. Moreover, as can be seen in Fig. 5 (g) - (h) ε increases with about 7% with decreasing t_o from 25 °C to 15 °C and with about 5% with increasing t_i from 40 °C to 50 °C. Where, ξ improves with 51% with decreasing t_o from 25 °C to 15 °C and with 25% with increasing t_i from 40 °C to 50 °C as shown in Fig. 5 (i) - (j).

Fig. 6 (a)-(b) illustrates the temperature contours for cold and hot water in flow direction at different t_i and t_o. As shown in Fig. 6 (a)-(b) the cold and hot regions retract and enlarge in flow direction for cold and hot water with increasing t_i and t_o, respectively. This is due to the increase of the heat transfer rate as a result of rising the temperature difference of cold/hot water flow through the coil.

Fig. 7 (a) - (f) illustrates the influences of Re_i and Re_o on Nu_i, Nu_o, P, and ε for a wide range of the variation of De_i and De_o. As shown in Fig. 7 (a)-(b), Nu_i, Nu_o, and P increase with increasing De_i and De_o, and ε decrease and increases with increasing De_i and De_o, respectively. The attributions of these trends are the same as discussed in Fig. 5. Moreover, Fig. 7 (a) shows that Nu_i slightly increases with increasing Re_o from 14,000 to 22,000, and this can be attributed to the increase of the turbulence level of cold water that dominates on the increase of water velocity that enhances the rate of heat transfer. On the other side, Nu_o slightly decreases with increasing Re_i from 9000 to 17,000 as displays in Fig. 7 (b), and this is due to the increase of hot water velocity that overcomes on the increase in the turbulence level and then the lower heat transfer is prevailed. Fig. 7 (c)-(d) shows that P increases with increasing Re_o and Re_i and this is due to the same explanation as discussed in Fig. 5 (e)-(f) where, the effects of Re_i and Re_o are the same of De_i and De_o since D_c, d and N are fixed. Additionally, the coil power consumption, P reduces with ≈31% by decreasing Re_o from 22,000 to 14,000 and decreases with ≈68% by decreasing Re_i from 17,000 to 9000.

Fig. 7(e)-(f) illustrates that ε increases with increasing Re_o and with decreasing Re_i. The possible explanation is the same as that discussed in Fig. 5 (g)-(h). Furthermore, the ε increases with ≈17% by increasing Re_o from 14,000 to 22,000 °C and with ≈29% by decreasing Re_i from 17,000 to 9000.

4.2. Effects of number of inner tubes and coil inclination

The Variations of the average hot and cold water Nusselt numbers; Nu_i *and* Nu_o, U_o, P, ε and ξ against the number of inner tubes (N) for different coil inclination angles, $\beta = 0°, 45°$ *and* $90°$ are shown in Fig. 8. Fig. 8 (a)-(b) shows that Nu_i and Nu_o increase slightly with increasing N from 1 to 3, and then decrease slightly with increasing N from 3 to 5 and the trend is the same at any β. Increasing N leads to: increasing the heat transfer surface area and consequently the heat transfer rate that causes higher temperature difference for hot and cold water along the coil and decreasing the temperature difference between hot/cold water and inner tubes surface; $\Delta t_{s,i,avg}$ *and* $\Delta t_{s,o,avg}$. The increase of Nu_i and Nu_o for $N < 3$ *is* attributed to the decrease of $\Delta t_{s,i,avg}$ and $\Delta t_{s,o,avg}$ and the increase of the heat flux due to overcoming the increase of the heat transfer rate over the heat transfer surface. But, the decrease of the heat flux dominates the reduction in $\Delta t_{s,i,avg}$ and $\Delta t_{s,o,avg}$ for $N > 3$ that leads to lower Nu_i and Nu_o. Moreover, Fig. 8 (c)-(d) show that U_o enhances and P rises with increasing N *and* the trend is the same at any β. Improving of U_o is due to enhancing the heat flux more that dominates the increase in Δt_{LMTD}, while rising P is owing to increasing the pressure drop in hot and cold water sides and due to the increase of hot water mass flow rate with increasing N. Also, it is observed that U_o enhances with 59%, 39% and 52% if N changed from 1 to 5 at β = 0°, 45° and 90°,

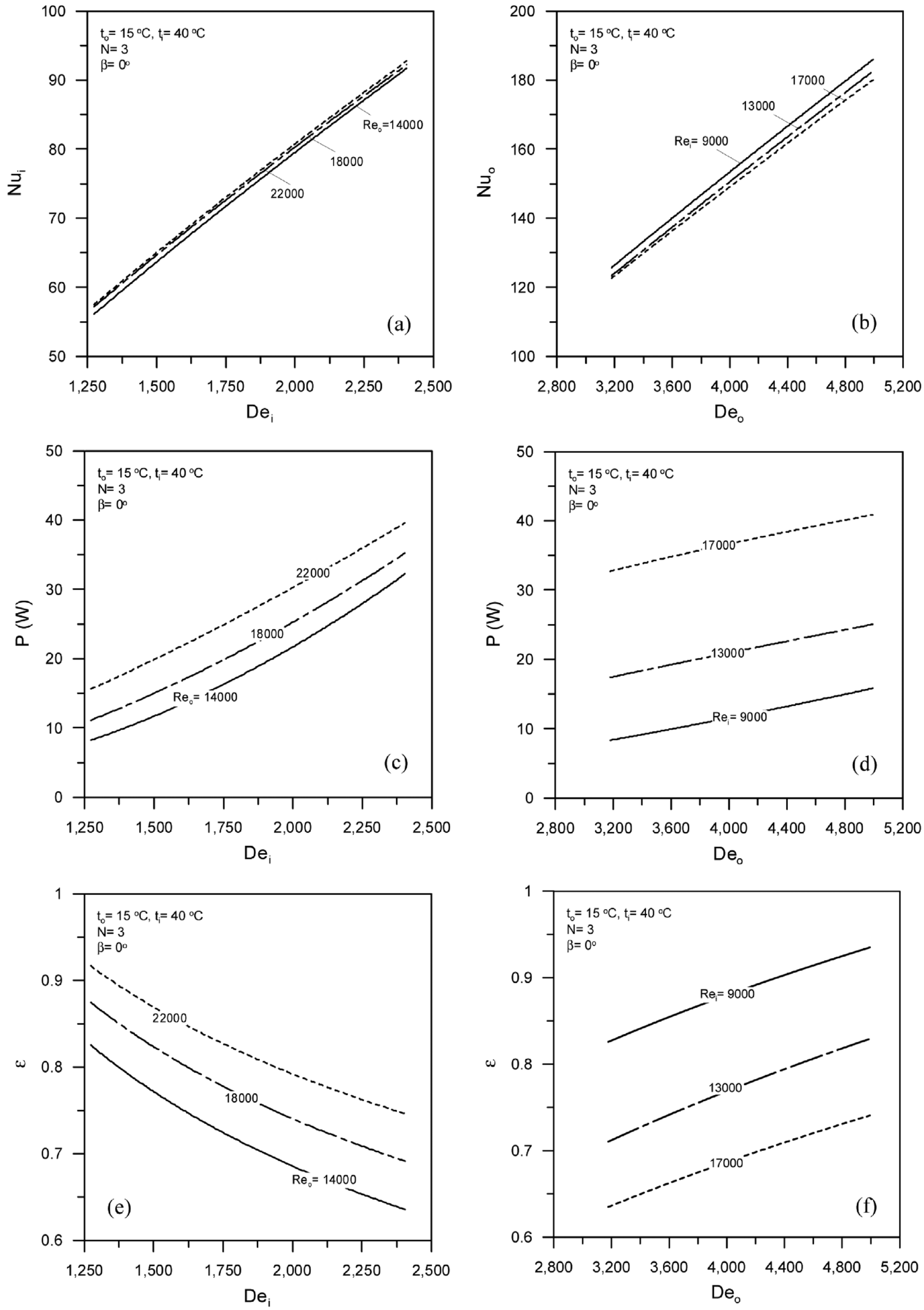

Fig. 7. Effect of hot/cold water Reynold's number on coil performance.

respectively and P rises with ≅20 times with increasing N from 1 to 5 at any β.

Furthermore, Fig. 8 (e) and (f) display that ε and ξ increase with increasing N from 1 to 3 and then they decrease for $N < 3$ and the same trend is observed at any β. Increasing ε with N (for $N > 3$) is due to rising the average heat transfer rate which dominates on the increase of the minimum heat capacity, i.e. higher amount of maximum possible heat transfer rate and vice versa for $N < 3$. Also, as can be seen, ε enhances with 8.5%, 9% and 7% if N increased from 1 to 3 at $\beta = 0°$, 45° and 90°, respectively. While, increasing ξ with N (for $N > 3$) is

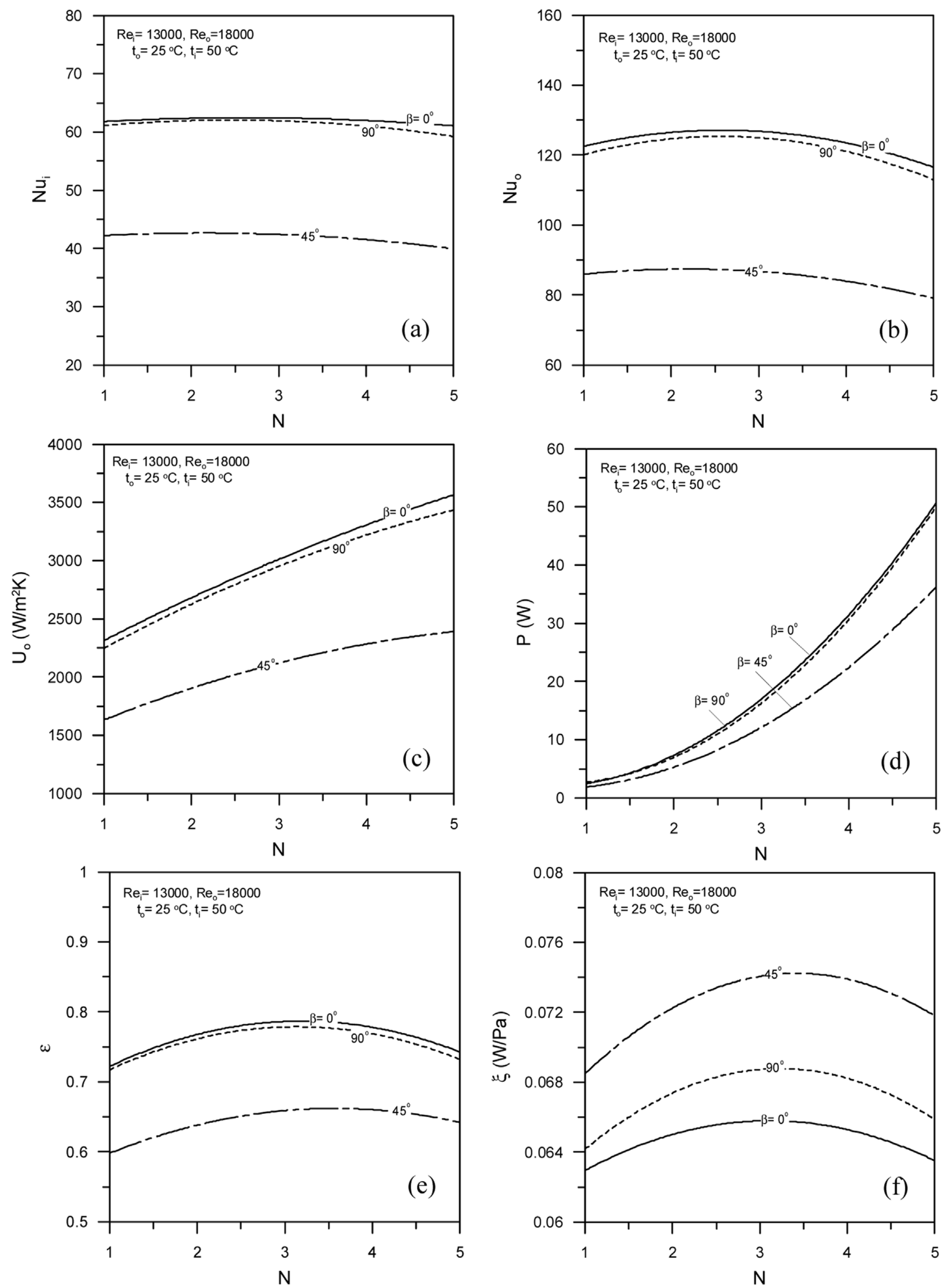

Fig. 8. Effect of number of inner tube on coil performance.

owing to overcoming the heat transfer rate over the pressure drop along the coil with increasing *N*, and vice versa for $N > 3$. The thermal-hydraulic index, ξ can be improved with 5%, 8% and 6% if *N* increased from 1 to 3 at $\beta = 0°$, 45° and 90°, respectively and its maximum value can be obtained at $\beta = 45°$.

Additionally, Fig. 8 displays that, Nu_i, Nu_o, U_o, P and ε have the largest values at $\beta = 0°$ *and* $90°$ and have the smallest values at $\beta = 45°$ and vice versa for ξ, and the same trend is appeared for any *N*, De_i *and* De_o. The possible explanation is due to the compound and opposite effects on the flow directions: (i) buoyancy force in upward direction and (ii) gravitational force in downward direction. In all the present simulations for all the studied ranges parameters the buoyancy parameter (*Bo*) is found less than 5.6×10^{-7} (criterion of onset the buoyancy effect that derived by Jackson et al. [28]) as a result of high

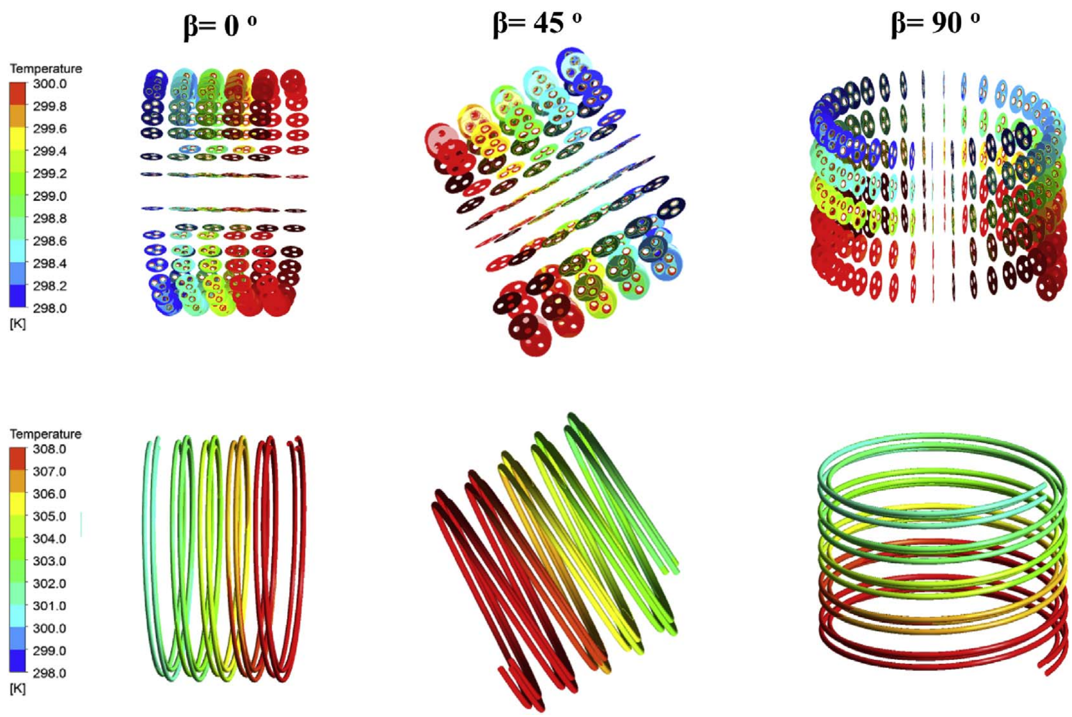

Fig. 9. Temperature contours at different coil inclination angles.

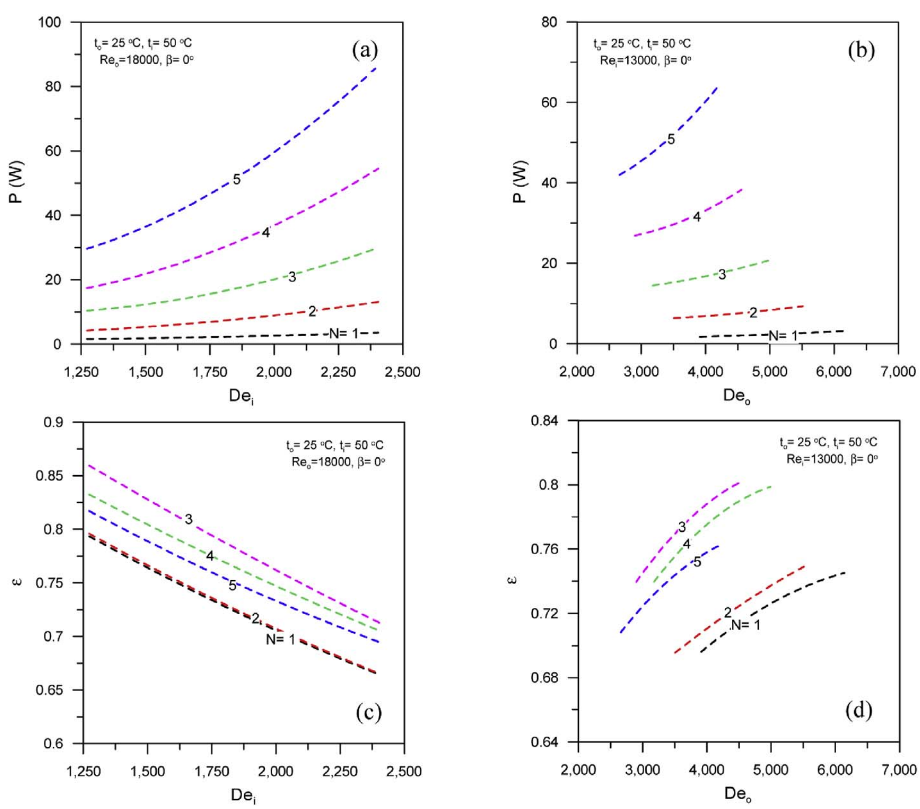

Fig. 10. Effect of number of inner tube on coil pumping power and effectiveness with different Dean numbers.

Reynold's numbers of single liquid phase flow so, the buoyancy force is negligible for the present simulation work. Nevertheless, the gravitational force has a significant effect on the coil inclination, thus the lower Nu_i, Nu_o, U_o, P and ε at $\beta = 45°$ is owing to the gravitational force component due to coil inclination that reduces the shear forces on the heat transfer surfaces. Hence the lower heat transfer rate and lower coil performance are obtained, but at β = 0° and 90° the coil experiences the same and higher performance, and vice versa for ξ.

Fig. 9 shows the temperature contours of hot and cold water flows at $Re_i = 13000$, $Re_o = 18000$, $t_i = 50$ °C, $t_o = 25$ °C and N = 3 for $\beta = 0°$, 45° and 90°. As shown in the figure the cold regions of the hot water in flow direction minimizes at $\beta = 45°$, and maximizes at β = 0° and 90°

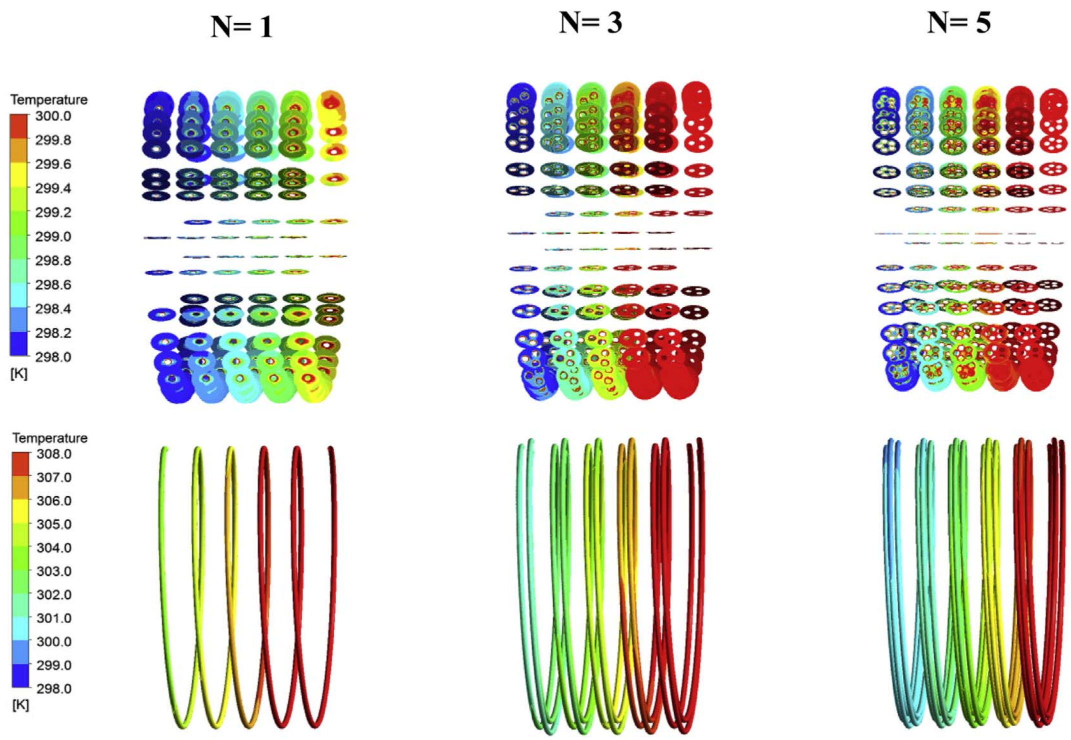

Fig. 11. Temperature contours at different number of inner tubes.

and vice versa for cold water flow. At $\beta = 45^{\circ}$ the heat transfer rate reduces as a result of lowering the gravitational and shear forces and consequently a decrease in the temperature difference along the coil for cold/hot water can be revealed.

Fig. 10 illustrates the effects of N on the pumping power, P and effectiveness, ε versus hot and cold water dean numbers, De_i and De_o respectively at $Re_i = 13000$, $Re_o = 18000$, $t_i = 50\,^{\circ}C$ and $t_o = 25\,^{\circ}C$. As shown in Fig. 10 (a) and (b), the pumping power (P) increases with increasing De_i and De_o and considerable increasing is observed with increasing N. This can be attributed to the increases of hot/cold water pressure drops and the flow rates with increasing the hot/cold water Reynold's numbers as explained in Figs. 5 and 7, that pressure drops and flow rates are magnified with increasing N. Also, it is observed in Fig. 10 (a) and (b) that P rises with 125%, 186% and 192% for N = 1, 3, and 5, respectively if De_i increases from 1273 to 2404, moreover, P rises with 52% if De_o increases from 2660 to 4180 for N = 5.

Fig. 11(c) and (d) show that ε drops and rises with increasing De_i and De_o, respectively and this trend is the same at any N. Decreasing ε with De_i is due to the increase of C_{min} with increasing Re_i which leads to higher $\dot{Q}_{max}$ and then lower ε, but increasing ε with De_o is owing to the increase of U_o which leads to higher heat transfer rate as discussed in Figs. 5 and 7. As shown in Fig. 11(c) and (d) the maximum effectiveness can be obtained at N = 3, where ε improves with 20% with dropping De_i from 2404 to 1273, and with 8.5% with increasing De_o from 2900 to 4556.

The temperature contours of hot and cold water flows at $Re_i = 13000$, $Re_o = 18000$, $t_i = 50\,^{\circ}C$, $t_o = 25\,^{\circ}C$ and $\beta = 0^{\circ}$ for N = 1, 3, and 5 are also illustrated in Fig. 11. As shown in the figure the cold and hot regions increase in flow direction for hot and cold water, respectively with increasing N. This is attributed to the increase of heat transfer surface area that enhances the cold/hot water heat transfer coefficients and consequently an increase in the temperature difference along the coil for cold/hot water can be appeared.

4.3. Numerical correlations

The numerical results are regressed to expect general numerical correlations for coil thermal and hydraulic performance measuring parameters; P, ε and ξ from all studied parameter ranges, see Table 1 for easy use of the present work results. Fig. 12 (a), (c) and (e) displays the developed correlations for P, ε and ξ, respectively in terms of De_i, De_o, Pr_i, Pr_o, N, and β (in degree), while Fig. 12 (b), (d), and (f) shows the predicted correlations errors. The developed correlations are given as follows:

Pumping power of the coil, P (W)

$$P(W) = (-4.6 \times 10^{-8}) De_i^{1.81} De_o^{0.71} \mathrm{Pr}_i^{0.39} \mathrm{Pr}_o^{0.39} N^{2.34} \times(-2.63 \times 10^{-3} + 3.2 \times 10^{-4}\beta - 3.48 \times 10^{-6}\beta^2) \quad (23)$$

Equation (23) can predict the majority of the simulated results (88%) within maximum error of ± 15%.

Effectiveness of the coil, ε

$$\varepsilon = 3.33 \times 10^{-2} \left(\frac{De_i}{De_o}\right)^{-0.36} \left(\frac{\mathrm{Pr}_i}{\mathrm{Pr}_o}\right)^{-0.61} N^{0.12} \times(194 - 2.8\beta + 3.06 \times 10^{-2}\beta^2)^{0.48} \quad (24)$$

Equation (24) can predict the majority of the simulated results (97%) within maximum error of ± 10%.

Thermal-hydraulic index, ξ (W/Pa)

$$\xi = 1.59 \times 10^{-3} \left(\frac{De_i}{De_o}\right)^{-0.99} \left(\frac{\mathrm{Pr}_i}{\mathrm{Pr}_o}\right)^{-3.46} N^{0.45} \times(35 - 0.14\beta + 1.8 \times 10^{-3}\beta^2)^{0.42} \quad (25)$$

Equation (25) can predict the majority of the simulated results (85%) within maximum error of ± 15%.

5. Conclusions

Thermal and hydraulic performance study for MTTHC heat exchanger using ANSYS-FLUENT 14.5 CFD code is conducted to investigate the cold/hot water Nusselt numbers, heat transfer coefficients, pumping power, effectiveness, and thermal-hydraulic index for turbulent flow. The effects of number of inner tubes, coil inclination angle, cold/hot water Reynolds/Dean numbers and temperatures on the coil thermal and hydraulic performance are fulfilled and discussed. The

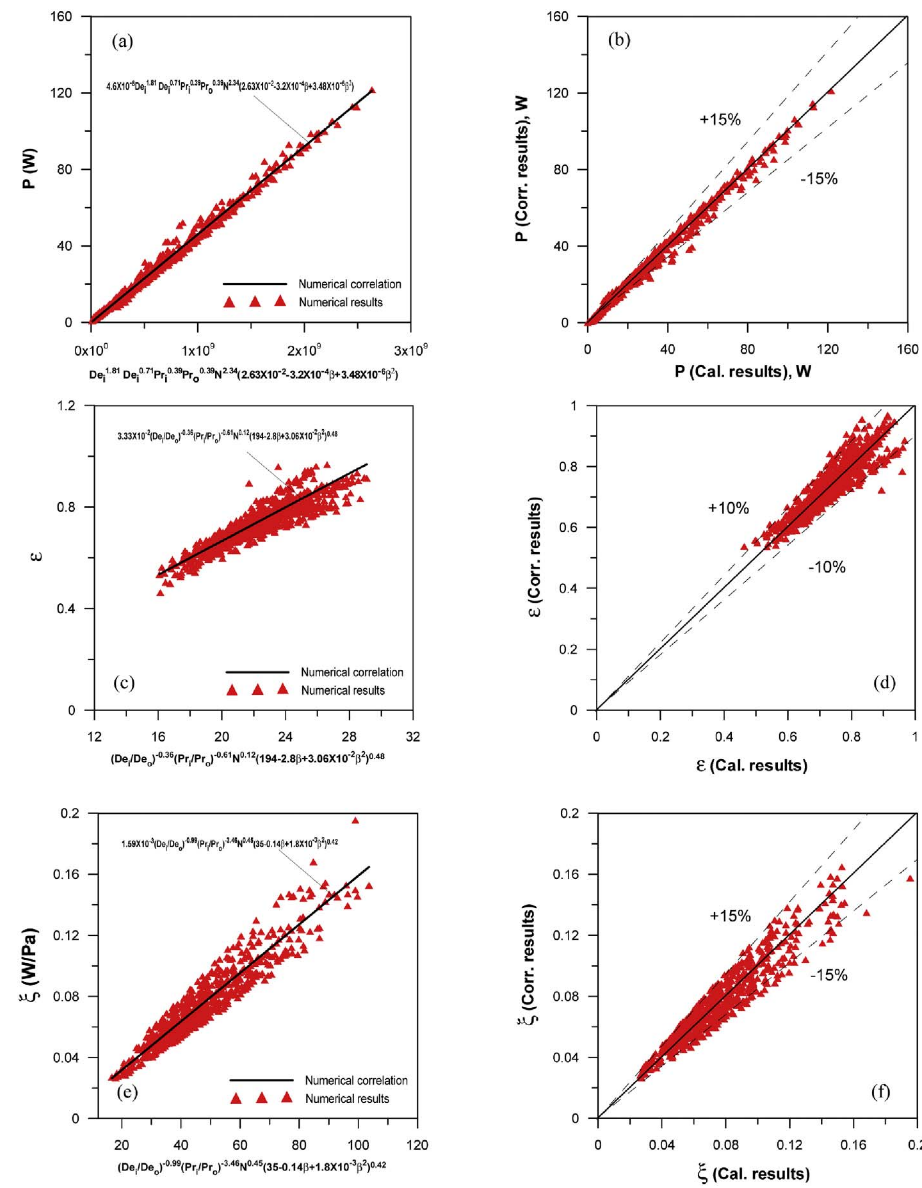

Fig. 12. Numerical correlations prediction and their errors.

main conclusions are given in the following:

Nu_i and Nu_o increase slightly with increasing N for N = 3 and decrease slightly for $N \geq 3$. Moreover, U_o enhances with increasing N and it has largest values at $\beta = 0^\circ$ *and* 90°, and the smallest value at $\beta = 45^\circ$ for any *N, De_i and De_o*. Where, U_o enhances with 59%, 39% and 52% and if *N* changed from 1 to 5 at $\beta = 0^\circ$, 45° and 90°, respectively.

Pumping power, *P* decreases with decreasing t_o, t_i, Re_o, Re_i, and N, where it has the smallest values at $\beta = 45^\circ$ and largest values at $\beta = 0^\circ$ *and* 90° for any *N, De_i and De_o.* Whereas, *P* reduces with $\approx 31\%$ by decreasing Re_o from 22,000 to 14,000 and with $\approx 68\%$ by decreasing Rei from 17,000 to 9000.

Additionally, *P* rises with ≅20 times if *N* changed from 1 to 5 at any β and *it* rises with 125%, 186% and 192% for N = 1, 3, and 5, respectively if De_i increases from 1273 to 2404, moreover, *P* rises with 52% if De_o increases from 2660 to 4180 for N = 5.

Effectiveness, ε and the thermal-hydraulic index, ξ decrease with increasing De_i, N ($N \geq 3$) and increases with increasing De_o, N (N = 3) for any t_i & t_o, β, moreover, ε has the largest values at $\beta = 0^\circ$ *and* 90° and *N=3,* and it has smallest value at $\beta = 45^\circ$ for any *N, De_i and De_o*. Where, ε improves with 20% with dropping De_i from 2404 to 1273, and with 8.5% with increasing De_o from 2900 to 4556. Also, ε increase with about 7% with decreasing t_o from 25 °C to 15 °C and with about 5% with increasing t_i from 40 °C to 50 °C. Additionally, ε increases with $\approx 17\%$ by increasing Re_o from 14,000 to 22,000 °C and with $\approx 29\%$ by decreasing Re_i from 17,000 to 9,000, and it enhances with 8.5%, 9% and 7% if *N* increased from 1 to 3 at $\beta = 0^\circ$, 45° and 90°, respectively. In other side, ξ improves with 51% with decreasing t_o from 25 °C to 15 °C and with 25% with increasing t_i from 40 °C to 50 °C, and it improves with 5%, 8% and 6% if *N* increased from 1 to 3 at $\beta = 0^\circ$, 45° and 90°, respectively and its maximum value can be obtained at $\beta = 45^\circ$. Finally, numerical correlations for pumping power, effectiveness and thermal-hydraulic index of the coil are correlated within reasonable errors.

References

[1] Xin RC, Ebadian MA. The effects of Prandtl numbers on local and average convective heat transfer characteristic in helical pipes. J Heat Tran 119:467–473.
[2] R.C. Xin, A. Awwad, Z.F. Dong, M.A. Ebadian, An experimental study of the single-phase and two-phase flow pressure drop in annular helicoidal pipes, Int J Heat Fluid Flow 18 (1997) 482–488.
[3] T.J. Rennie, V.G.S. Raghavan, Experimental studies of a double-pipe helical heat exchanger, Exp Therm Fluid Sci 29 (2005) 919–924.
[4] Vimal Kumar, Supreet Saini, Manish Sharma, K.D.P. Nigam, Pressure drop and heat transfer study in tube-in-tube helical heat exchanger, Chem Eng Sci 61 (2006)

4403–4416.
[5] Vimal Kumar, Burhanuddin Faizee, Monisha Mridha, K.D.P. Nigam, Numerical studies of a tube-in-tube helically coiled heat exchanger, Chem Eng Process 47 (2008) 2287–2295.
[6] J.S. Jayakumar, S.M. Mahajani, J.C. Mandal, P.K. Vijayan, Rohidas Bhoi, Experimental and CFD estimation of heat transfer in helically coiled heat exchangers, Chem Eng Res Des 86 (2008) 221–232.
[7] Ivan Di Piazza, Michele Ciofalo, Numerical prediction of turbulent flow and heat transfer in helically coiled pipes, Int J Therm Sci 49 (2010) 653–663.
[8] D. Colorado, D. Papini, J.A. Hernández, L. Santini, M.E. Ricotti. Development and experimental validation of a computational model for a helically coiled steam generator.
[9] Yuanyuan Zhou, Jianlin Yu, Xiaojuan Chen, Thermodynamic optimization analysis of a tube-in-tube helically coiled heat exchanger for JouleeThomson refrigerators, Int J Therm Sci 58 (2012) 151–156.
[10] S.A. Nada, EI Eid, G.B. Abd El Aziz, H.A. Hassan, Performance enhancement of shell and helical coil water coolers using different geometric and fins conditions, Heat Tran Asian Res 45 (7) (2016) 631–647.
[11] E. Amori Karima, Thermal and hydraulic characteristics of a novel helical coiled tube used as a heat exchanger, Arabian J Sci Eng 39 (2014) 4179–4186.
[12] S.A. Nada, W.G. El Shaer, A.S. Huzayyin, Heat transfer and pressure drop characteristics of multi tubes in tube helically coiled heat exchanger, JP J Heat Mass Transf 9 (2014) 173–202.
[13] S.A. Nada, W.G. El Shaer, A.S. Huzayyin, Performance of multi tubes in tube helically coiled as a compact heat exchanger, Heat Mass Tran 51 (2014) 973–982.
[14] S.A. Nada, H.F. Elattar, A. Fouda, H.A. Refaey, Numerical investigation of heat transfer in annulus laminar flow of multi tubes-in-tube helical coil, Heat Mass Tran (2017), http://dx.doi.org/10.1007/s00231-017-2163-8.
[15] A. Fouda, S.A. Nada, H.F. Elattar, H.A. Refaey, A. Bin Mahfouz, Thermal performance Modelling of turbulent flow in multi tubes in tube helically coiled heat exchangers, Int J Mech Sci 135 (2018) 621–638.
[16] S.S. Pawar, VivekK, Sunnapwar, Experimental and CFD investigation of convective heat transfer in helically coiled tube heat exchanger, Chem Eng Res Des 92 (2014) 2294–2312.
[17] Changzhao Pan, Yuan Zhou, Junjie Wang, CFD study of heat transfer for oscillating flow in helically coiled tube heat-exchanger, Comput Chem Eng 69 (2014) 59–65.
[18] B.K. Hardik, P.K. Baburajan, S.V. Prabhu, Local heat transfer coefficient in helical coils with single phase flow, Int J Heat Mass Tran 89 (2015) 522–538.
[19] M. Sartori, D.S. Oliveira, E.C. Teixeira, W.B. Rauen, N.C. Reis Jr., CFD modelling of helically coiled tube flocculators for velocity gradient assessment, J Braz Soc Mech Sci Eng 37 (2015) 187–198.
[20] S.S. Pawar, V.K. Sunnapwar, A.R. Tagalpallewar, Development of experimental heat transfer correlations using Newtonian fluids in helical coils, Heat Mass Tran 52 (2016) 169–181.
[21] H. Bahremand, A. Abbassi, M. Saffar-Avval, Experimental and numerical investigation of turbulent nanofluid flow in helically coiled tubes under constant wall heat flux using Eulerian–Lagrangian approach, Powder Technol 269 (2015) 93–100.
[22] Wandong Zheng, Tianzhen Ye, Shijun You, Huan Zhang, The thermal performance of seawater-source heat pump systems in areas of severe cold during winter, Energy Convers Manag 90 (2015) 166–174.
[23] Wandong Zheng, Huan Zhang, Shijun You, Tianzhen Ye, Numerical and experimental investigation of a helical coil heat exchanger for seawater-source heat pump in cold region, Int J Heat Mass Tran 96 (2016) 1–10.
[24] Wandong Zheng, Tianzhen Ye, Shijun You, Huan Zhang, Xuejing Zheng, Experimental investigation of the heat transfer characteristics of a helical coil heat exchanger for a seawater-source heat pump, J Energy Eng 142 (1) (2016).
[25] Wandong Zheng, Huan Zhang, Shijun You, Tianzhen Ye, The thermal characteristics of a helical coil heat exchanger for seawater-source heat pump in cold winter, Procedia Engineering 146 (2016) 549–558.
[26] T.H. Shih, A. Shabbir, J. Zhu, A new k-ε eddy-viscosity model for high Reynolds number turbulent flows - model development and validation, Comput Fluids 24 (3) (1995) 227–238.
[27] J.P. Holman, W.J. Gajda, Experimental method for engineering, McGraw Hill, New York, 1989.
[28] J.D. Jackson, M.A. Cotton, B.P. Axcell, Studies of mixed convection in vertical tubes, Int J Heat Fluid Flow 10 (1989) 2–15.